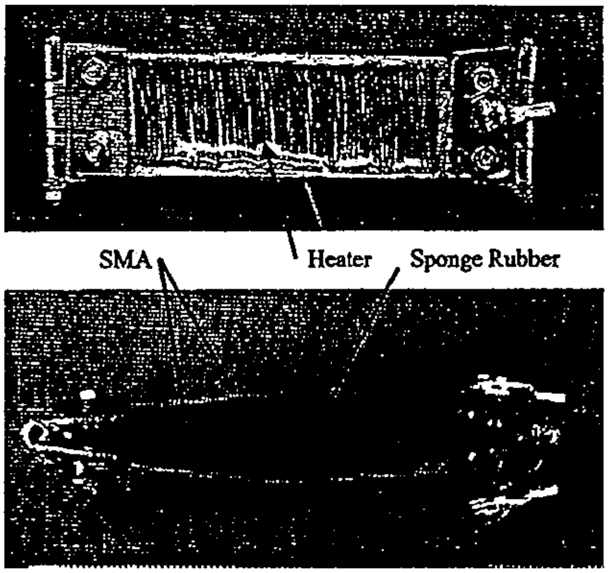

FIG. 9. Shown is a prototype artificial sphincter.

We developed an artificial sphincter to meet this need using an SMA to the stoma as shown in Fig. 9 (4). When the temperature is raised by electricity, the artificial sphincter opens, which allows patients to control their evacuations. A photograph of a prototype artificial sphincter is shown in Fig. 9. Long-term animal experiments are now being conducted on this device.

Electric power was supplied to the artificial sphincter by the use of the transcutaneous energy transmission system (TETS) as shown in Fig. 4.

Basic performance of this artificial implantable device is now under discussion. However, we are still evaluating different coating materials for the implantable part, because Silastic material for an implantable device is difficult to import.

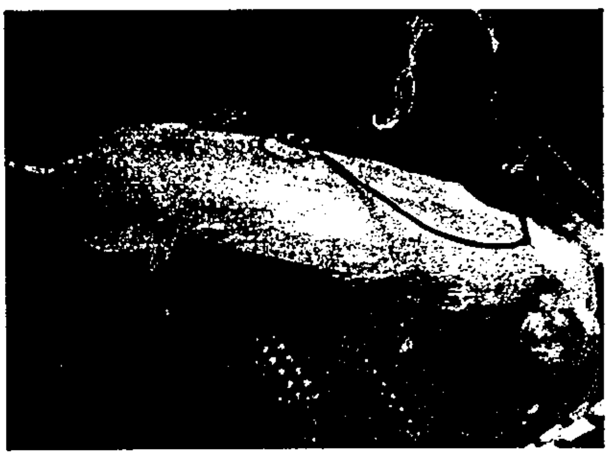

FIG. 10. A pig with artificial sphincter is shown.

The objective of the design concept is to enable patients to go to the bathroom whenever they choose. And then, when ready, they would take the TETS and attach it to their abdomen so that they would be able to control the implanted sphincter easily.

At present, the development of an artificial sphincter is at the stage of long-term animal experiments. Figure 10 shows a pig with a stoma and artificial sphincter. We are currently conducting a long-term endurance test for an artificial sphincter with TETS. When this test is completed we aim to begin preclinical trials.

CONCLUSION

This article reports on various artificial organs developed by Tohoku University and evaluates them for clinical applications.

Acknowledgments: The authors thank Mr. Kimio Kikuchi for experimental preparation and kind cooperation, and Miss Yoko Ito and Mrs. Hisako Iijima for their excellent technical assistance and kind cooperation.

This work was partly supported by a Grant-in-aid for Scientific Research (11480253), Research Grant for Cardiovascular Diseases from the Ministry of Health, Labour and Welfare, Program for Promotion of Fundamental Studies in Health Science of Organizing for Drug ADR Relief, R&D Promotion and Product Review of Japan, and Health and Labour Science Research Grant for Research on Advanced Medical Technology.

REFERENCES

1. Sawyer PN, Page M, Rudewald B, Baselius L, McCool C, Lester E, Stanzwski B, Srinivasan S, Ramasamy N. Further study of NITINOL wire as contractile artificial muscle for an artificial heart. Cardiovasc. Diseases Bull Tex. Heart Inst 3;65:1976.
2. Hayashi K, Seki J, Nakamura T. Application of shape memory alloys to the actuator of the artificial heart. Iyodenshi To Seitai Kogaku 23(1):1985;1–6 (in Japanese).
3. Nitta S, Takahasi A, Katahira Y, Tanaka M, Okamoto T, Kagawa K, Hongo T, Watanabe T, Horiuchi T, Tanji A, Yamauchi K, Yabuki T. Application of shape memory alloy for an artificial heart driving system. MBE 83–49;45–51:1983 (in Japanese).
4. Amae S, Wada M, Luo Y, Nakamura H, Yoshida S, Kamiyama T, Yambe T, Takagi T, Nitta S, Ohi R. Development of an implantable artificial anal sphincter by the use of the shape memory alloy. *ASAIO J* 2001;47(4):346–50.
5. Tanaka M, Hirano K, Goto H, Namima T, Uchi K, Jiang ZW, Matsuki H, Tanahashi Y, Orikasa S, Chonan S. Artificial SMA valve for treatment of urinary incontinence: Upgrading of valve and introduction of transcutaneous transformer. *Biomed Mater Eng* 1999;9:97–112.
6. Snyder AJ, Rosenberg G, Reibson J, Donachy JH, Prophet GA, Arenas J, Daily B, McGary S, Kawaguchi O, Quinn R,

Pierce WS. An electrically powered total artificial heart: Over 1 year survival in the calf. *ASAIO J* 1992;38:M707–12.
7. Yambe T, Owada N, Kobayashi S, Sonobe T, Naganuma S, Nanka S, Hashimoto H, Yoshizawa M, Tabayashi K, Takayasu H, Takeda H, Nitta S. Left heart bypass using the oscillated blood flow with totally implantable vibrating flow pump. *Artif Organs* 1998;22:426–9.
8. Kung RTV, Yu RS, Ochs BD, Parnis SM, Macris MP, Frazier OH. Progress in the development of the ABIOMED total artificial heart. *ASAIO J* 1995;41:M245–8.
9. Nojiri C, Kijima T, Maekawa J, Horiuchi K, Kido T, Sugiyama T, Mori T, Sugiura N, Asada T, Shimane H, Mishimura K, Ban T, Akamatsu T, Ozaki T, Ito H, Suzuki M, Akutsu T. More than 1 year continuous operation of a centrifugal pump with a magnetically suspended impeller. *ASAIO J* 1997;43:M548–52.
10. Yambe T, Nitta S, Sonobe T, Naganuma S, Kobayashi S, Yoshizawa M, Fukutome A. Development of total artificial heart having advantages in economy and durability. *Int J Artif Organs* 1998;21:279–84.
11. Tatsumi E, Nakamura M, Masuzawa T, Taenaka Y, Sohn YS, Nishimura T, Nakata M, Nakatani T, Ohno T, Endo S, Takiura K, Takewa Y, Kakuta Y, Takano H. In vitro and in vivo evaluation of a left-right balancing capacity of an interatrial shunt in an electrohydraulic total artificial heart system. *ASAIO J* 1997;43:M619–25.
12. Takagi T, Lu Y, Hara S, Yambe T, Amae S, Wada M, Nakamura H. Artificial Sphincter using Shape Memory Alloy Actuators. Digest for Invited Speakers and Referees of the 3rd Japan-France Seminar on Intelligent Materials and Structures. 2000; 180–5.

Open-loop Analysis of Transfer Characteristics from Blood Pressure to Heart Rate Using an Effectively Total Artificial Heart

*Akira Tanaka, †Makoto Yoshizawa, *Ken-ichi Abe, ‡Hiroshi Takeda, §Tomoyuki Yambe, §Shin-ichi Nitta, ¶Yusuke Abe, ¶Tsuneo Chinzei, and ¶Kou Imachi

*Department of Electrical and Communication Engineering, Graduate School of Engineering, Tohoku University, Sendai; †Research Division on Advanced Information Technology, Information Synergy Center, Tohoku University, Sendai; ‡Department of Electrical Engineering, Faculty of Engineering, Tohoku Gakuin University, Tagajo; §Department of Medical Engineering and Cardiology, Institute of Development, Aging and Cancer, Tohoku University, Sendai; ¶Graduate School of Medicine, University of Tokyo, Tokyo, Japan

Abstract: It is desirable for the dynamic behavior of the drive rate of the artificial heart to be as similar as possible to that of the recipient's heart rate (HR) before implantation. This requires a model which can simulate the behavior of HR on the basis of only the information measured with the limited number of approvable implanted sensors. This article provides a linear time series model for explaining the behavior of HR only with aortic pressure and right atrial pressure. This could be obtained from open-loop analysis using a total artificial heart, which was introduced for measuring HR in vivo and for eliminating its effect on blood pressure. The model was identified in a goat equipped with a special biventricular assist device called the effectively total artificial heart (ETAH). The ETAH was introduced to make an open loop and awake situation in the animal with almost intact autonomic nerves, which could enhance the accuracy and reliability of the identification of the model. The adequacy of the proposed model was ascertained in several data sets measured in two goats, which were different from the data set used for identification. Most of the mean estimation errors were less than 3 beats/min and auto-correlation analysis showed approvable statistical appropriateness. However, it was clarified through comparison with the 1/R control method that the proposed model has a few problems still to be solved before its future implementation as an automatic controller of the TAH. **Key Words:** Heart rate variability—Total artificial heart—Peripheral vascular resistance—System identification—Autoregressive exogenous model.

Received August 2001; revised March 2003.

Address correspondence and reprint requests to Dr. Akira Tanaka, Department of Electrical and Communication Engineering, Graduate School of Engineering, Tohoku University, Aoba-yama 05, Sendai 980-8579, Japan. E-mail: tanaka@abe.ecei.tohoku.ac.jp

INTRODUCTION

One of the most important problems in controlling the total artificial heart (TAH) is how we should determine the cardiac output, i.e., the flow pumped out from the TAH to the vascular system. Although many methods for solving this problem have been proposed, no decisive methods have yet been found (1–4).

We may have two keys to solving this problem. One key is to clarify the total mechanism of the cardiovascular center determining the cardiac output. However, even if the mechanism is completely clarified, we will not be able to implement a controller with a similar mechanism because we can only measure a small part of the physiological information, while the cardiovascular center can use the whole information. The other key is to mimic the dynamic behavior of the cardiovascular center for regulating the cardiac output on the basis of the limited number of measurements that we can obtain in the realistic situation.

One of the simplest methods for simulating the dynamic behavior of the cardiovascular center is to create a controller so that the drive rate (DR) of the TAH can behave as similarly as possible to the recipient's heart rate (HR) on the basis of only the information measured with the limited number of approvable sensors. This requires a certain mathematical model which can express the dynamics of HR variability and an assumption that the stroke volume can be regarded as being constant.

The "1/R control method" proposed by Abe et al. (5) is a candidate of such mathematical models representing the behavior of the HR. In this method, the DR at the next step is determined as a function of the current DR, aortic pressure (AoP) and right atrial pressure (RAP), subject to a constant stroke volume regulated by an automatic controller. This method could achieve the long survival of animals equipped with TAHs driven by the fully automatic controller. However, the method requires a searching process of a control parameter depending on individual differences and external conditions, such as the response time of the pump output. This process prevents us from applying the method to clinical use because the process must be done in a trial and error manner.

The substantial feedback information used by the 1/R method must be included in the AoP and RAP. Thus, it may be possible to find another, better model which can simulate the dynamic behavior of the HR as a function of these pressures.

One of the simplest methods for finding such a model is to apply the system identification technique to the dynamic system from AoP and RAP to the HR. In the case of an awake animal or human, however, this identification is not easy because the cardiovascular system is a closed-loop system, i.e., the HR is fed back to vascular pressures. Theoretically, it is proved that we should make the closed-loop system open to identify its subsystems as accurately as possible (8,9). However, it will, of course, be difficult to directly cut the feedback loop, for example by blocking autonomic nerves, unless we introduce some special experimental conditions to maintain the subject's blood perfusion (8,9).

To realize an approximately open-loop situation, in this study, a special animal model equipped with a kind of biventricular bypass system, called an *effectively total artificial heart* (ETAH), has been introduced, as shown in the next section.

The ETAH can be expected to provide an accurate identification of the system from blood pressures to the HR because the ETAH enables us to observe the HR under conditions in which the HR has little effect on the blood pressure, in spite of an awake animal with an intact autonomic nervous system.

METHODS

Animal experiment

Figure 1 shows a schematic illustration of the animal experiment using the ETAH. Two pneumatically-driven blood pumps (TH-7, Tohoku University, Japan) were used as a biventricular bypass, withdrawing blood from the right and left atria and transfusing it to the pulmonary artery and the aorta, respectively. The right pump bypassed 100% of blood flow of the right ventricle and the left pump bypassed about 80% of that of the left ventricle by clamping the ascending aorta. Thus, the effect of the HR on blood pressure could be sufficiently reduced while the HR still remained because the coronary circulation was maintained by the rest, about 20%, of the systemic circulatory flow. This situation could be regarded as nearly open loop because the paths from the HR to blood pressures were nearly cut off. However, the HR was still determined by the cardiovascular center, depending on the artificial variation of blood pressures driven by the two blood pumps.

In the experiment, two adult goats were employed to apply the ETAH. The HR was obtained from ECG, measured with electrodes implanted at the pericardium. The AoP and RAP were measured using pressure transducers through fluid-filled side catheters at the outlet port of the left pump and the intake port of the right pump, respectively.

After implantation, the ETAH was manually controlled so that blood flow and pressure could be on roughly normal physiological levels. Because the circulation had been unstable immediately after the operation, data acquisition was started a week later. ECG, AoP, RAP and the drive signal of the ETAH were measured at 500 Hz on a personal computer with an A/D converter. The DR and HR were obtained from processing the drive signal and ECG, respectively. The AoP and RAP were averaged over a drive period of the ETAH, and their averaged values and the DR were recorded at every drive beat. Independent of these values, the HR was recorded at every natural heartbeat.

To keep the characteristic of the persistent excitation (10) for increasing identifiability, the DR was randomly changed according to a rectangular signal, as shown in Fig. 2(a).

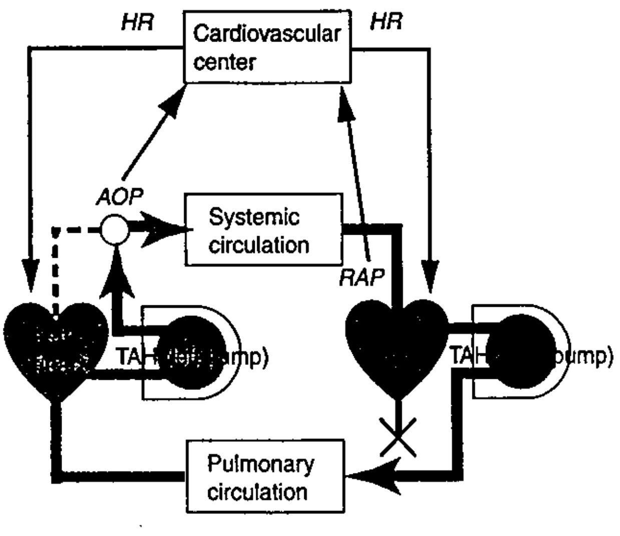

FIG. 1. A schematic illustration of animal experiments.

Data processing and system identification

It is necessary to sample at a fixed rate to identify the system dynamics. Therefore, each beat-to-beat data series was resampled at 2 Hz after smoothing by means of the cubic spline function because the maximum drive rate was less than 120 bpm. Then the time series data was linearly detrended and normalized to have zero mean and unit variance.

To estimate coefficient parameters and delays, the cross-correlation coefficients between the AoP and the HR, and the RAP and the HR were calculated.

The model of the HR regulator was indicated as a general linear model. According to the general process of system identification, the autoregressive exogenous (ARX) model, which can be estimated easily, was selected as follows:

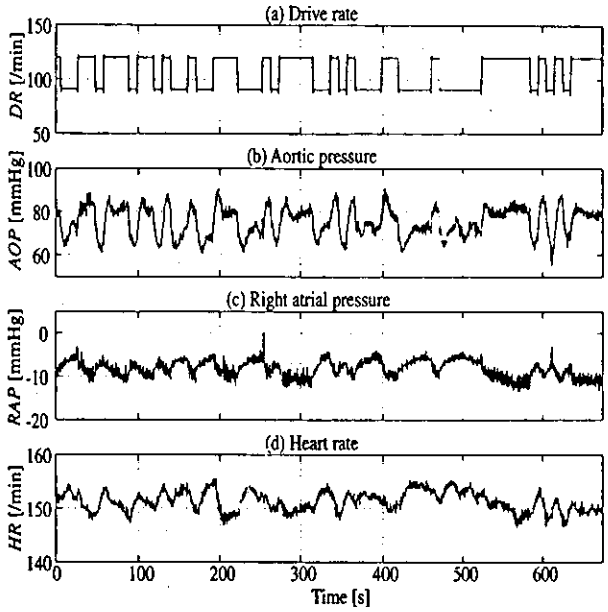

FIG. 2. The variation of *DR*, *AOP*, *RAP* and *HR* with time.

$$HR_k = \sum_{i=1}^{n} a_i HR_{k-i} + \sum_{j=0}^{m_{AOP}} b_j AOP_{k-L_{AOP}-j} + \sum_{l=0}^{m_{RAP}} c_l RAP_{k-L_{RAP}-l} + e_k \quad (1)$$

where HR_k, AOP_k and RAP_k are sampled values of the HR, AoP and RAP, respectively, and n, m_{AOP} and m_{RAP} are orders of HR_k, AOP_k and RAP_k, respectively. L_{AOP} and L_{RAP} are delays from AOP_k to HR_k and from RAP_k to HR_k, respectively. e_k is a residue.

First, L_{AOP} and L_{RAP} were determined from the first peak of the cross-correlation coefficient, and then all of the combinations in which the order of each parameter was from 1 to 10 were fitted to the data set with the chosen delays. The total number of models was 1000. For each of these models, the sum of the squared prediction errors and the resulting loss functions (normalized sum of the squared prediction errors) were computed. n, m_{AOP} and m_{RAP} were chosen such that the structure could have the smallest loss function.

Evaluation of identified models

To ascertain the adequacy of identified models, the output of the model was compared with measured data by using the following data sets.

A. The same data set as that used for the identification obtained from a goat.
B. Another data set obtained from the same goat as data set A in a different interval.
C. The data set obtained from another goat for which the DR was changed according to a random rectangular signal.
D. The data set obtained from the same goat as data set C for which the DR was kept constant.
E. The data set obtained from a goat not equipped with blood pumps but with only sensors, while 10 mg methoxamine hydrochloride was injected for changing blood pressure.

Data sets A and B were used to evaluate the adequacy of the parameter estimation. Data sets C–E were used to evaluate generality for individual differences. It is important to use data set E because the situation of the goats equipped with the ETAH may be very special.

If the system is correctly described, then the residuals associated with the data and a given model will ideally be white and independent of the input given to the model (10). To check these characteristics, the auto-correlation function of e_k and the cross-correlation function between e_k and the inputs, AOP_k and RAP_k, were computed.

RESULTS

Figure 2 shows an example of the time series data. It can be seen that the HR_k changed depending on variations of AOP_k and RAP_k caused by the change in DR_k. However, it can be considered that AOP_k and RAP_k were only slightly affected by HR_k because HR_k seemed to change to suppress the variation of these pressures, that is, HR_k increased with decreasing AOP_k and with increasing RAP_k, and vice versa. This implies that the baroreflex function of the cardiovascular center expressed in HR_k could work normally, even under almost the same condition as the TAH.

Figure 3(a,b) show the examples of the cross-correlation coefficients between AOP_k and HR_k and between RAP_k and HR_k, respectively. Note that HR_k is strongly correlated with AOP_k and RAP_k. The average lags at which the coefficients achieve their maximum are 5 s (the 10th sample) for AOP_k and 2.5 s (the 5th sample) for RAP_k.

As a result, L_{AOP} and L_{RAP} in Eq. 1 were chosen as follows:

$$L_{AOP} = 10,\ L_{RAP} = 5. \quad (2)$$

Then, after computing the loss function using Eq. 2, the orders of Eq. 1, n, m_{AOP} and m_{RAP}, were chosen as follows:

$$n = 2,\ m_{AOP} = 2,\ m_{RAP} = 2. \quad (3)$$

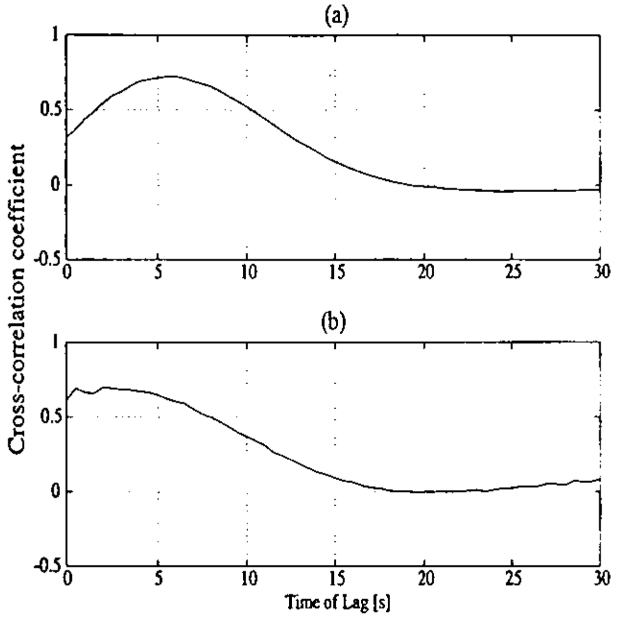

FIG. 3. The cross-correlation coefficient (a) from $-AOP_k$ to HR_k, and (b) from RAP_k to HR_k.

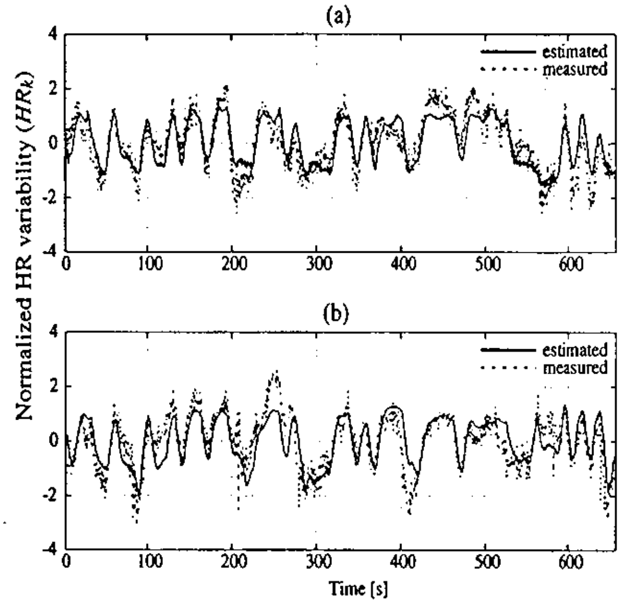

FIG. 4. The variation of the measured HR_k and its estimate for (a) data set A, and (b) data set B.

Finally, the parameters of the model were estimated using the least-squares method. Hence, Eq. 1 is expressed as follows:

$$\begin{aligned} HR_k = {} & 0.32HR_{k-1} + 0.48HR_{k-2} - 0.19AOP_{k-10} \\ & - 0.08AOP_{k-11} + 0.10RAP_{k-6} \\ & + 0.02RAP_{k-7} + e_k. \end{aligned} \tag{4}$$

Figure 4(a,b) show the variations of HR_k and its estimate with time. The estimates of Fig. 4(a,b) were calculated from data sets A and B, respectively. It can be seen that the linear model could estimate HR variability well, mainly at low frequencies up to the respiratory rate. The root-mean-squared value of the estimation error e_k was less than 2.0 beats/min.

Figure 5(a) shows the result of HR estimation in which the input data set was measured on a different goat from Fig. 4 (data set C). It can also be seen that the slow variation of HR is similar to the change in HR_k with AOP_k caused by the change in DR_k. The mean estimation error was less than 3.2 beats/min.

Figure 5(b) shows the result of the estimation in which the input data set was measured on the same goat as that of data set C but DR_k was kept constant (data set D). Hence, the change in AOP_k was not caused by the change in DR_k but in the characteristic of the systemic circulation and/or venous return. The estimation error was less than 3.1 beats/min.

Figure 6 shows the estimation results in which the input data set was measured on the different goat from Figs. 4 and 5, not equipped with blood pumps but with only sensors (data set E). In this data set, AOP_k was changed by injection of methoxamine hydrochloride (10 mg) at $t = 100$ s.

The auto-correlation function of e_k, the cross-correlation function between AOP_k and e_k, and the cross-correlation function between RAP_k and e_k are shown in Fig. 7(a,b,c), respectively. In each figure a 99% confidence interval, represented by dotted lines, is used to ensure that the residue e_k is indeed white and independent of the inputs. Almost all functions

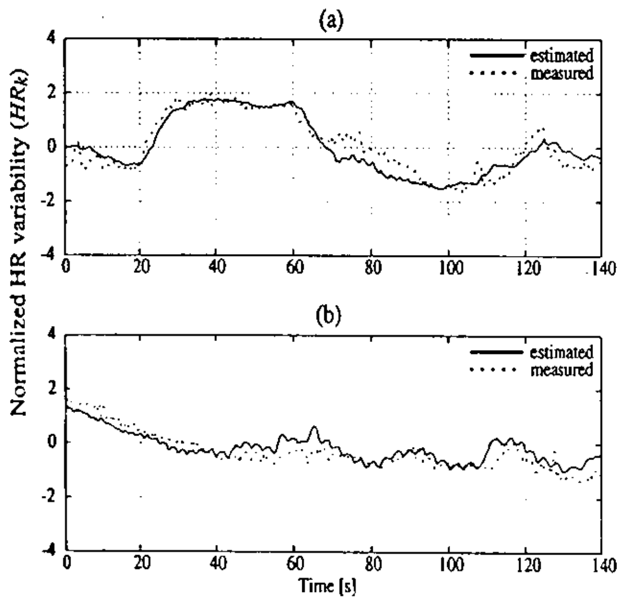

FIG. 5. The variation of the measured HR_k and its estimate for (a) data set C, and (b) data set D.

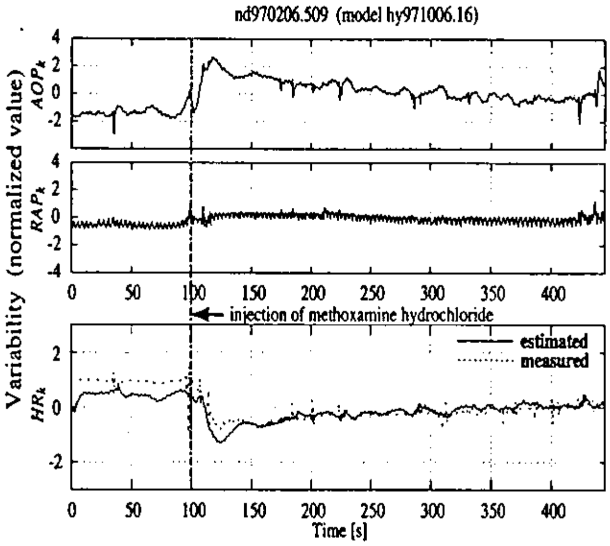

FIG. 6. The variation of the measured HR_k and its estimate based on data set E.

stay inside the interval, except for a few lag points. This result shows that the estimated model expressed by Eq. 4 may be statistically appropriate.

DISCUSSION

The present results of animal experiments have shown that the response of the HR to two kinds of blood pressures caused by the baroreflex function still remained under the awake and open-loop condition produced by the ETAH. Sugimachi et al. (8) and Kawada et al. (9) have already revealed the transfer function from the arterial pressure to the autonomic nervous activity under an open-loop condition in rabbits. However, these animals were anesthetized and their autonomic nerves were not perfectly intact. Moreover, the effect of preload was not considered because atrial pressure has never been analyzed.

As shown in Fig. 3, the values of the two delays, one is from the AoP to the HR and the other is from RAP, were different from each other. This suggests that the HR regulator has at least two control loops. One works depending on the afterload of the left heart and the other on the preload of the right heart. This indicated that the AoP and RAP should be fed back to the DR of the TAH with different delays rather than the same delay.

On the other hand, the 1/R control method manipulates the DR on the basis of the AoP and RAP with the same delay. Thus, the method leaves room for improvement, at least in adjusting delays in feedback loops.

The results of Figs. 4–6 mean that the identified ARX model could simulate the dynamic behavior of the HR at low frequencies up to respiratory rate, even in the three cases where the model was applied to different data sets obtained from the same goat, the different goat equipped with the ETAH and the different goat without the ETAH. Moreover, Fig. 6 suggests that it is possible to use the ARX model for estimating the HR to some extent on the basis of constant coefficient parameters, even when the peripheral vascular resistance is considerably changed.

This characteristic is important because it means that the functional relationship between blood pressures and the HR is roughly robust to the change in the peripheral vascular resistance and individual difference. It is a matter of course that this robustness is also desirable for general application of the automatic controller for the TAH because the structure or the parameters of the function determining the DR should be invariant for different hemodynamic states or different recipients.

As shown in Fig. 7, the results of the residual analysis showed statistical appropriateness of the identified ARX model. Thus, we cannot expect to improve the estimation accuracy any more as long as we use linear ARX models whose inputs are only the AoP and RAP.

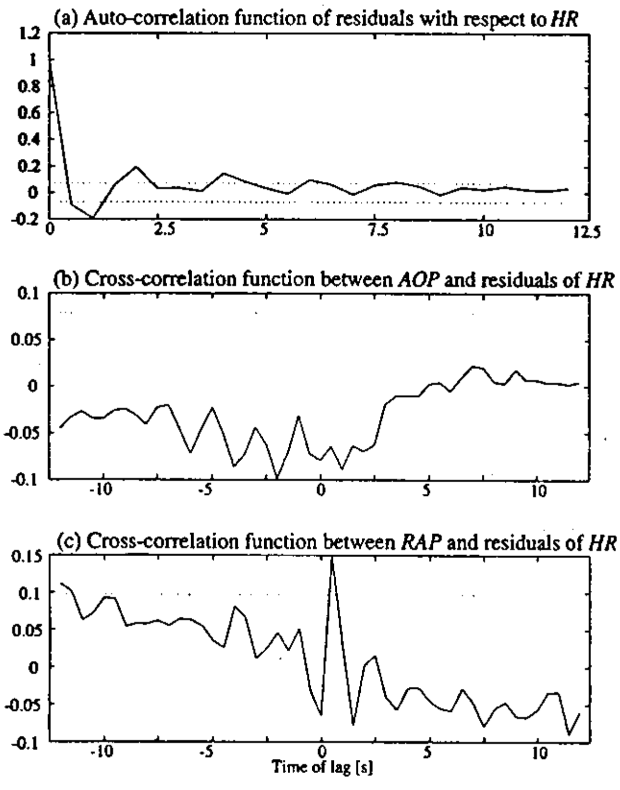

FIG. 7. The results of the residual analysis with respect to e_k.

However, this does not deny the existence of other better models with other additional kinds of inputs, for example, metabolic products (11) or the respiratory rate. In particular, the introduction of the respiratory rate may improve the estimation accuracy at high frequencies, which could not be estimated by the proposed model because it is well known that the HR variability has a high frequency component related to respiratory arrhythmia. However, its usefulness and significance are still unknown.

Furthermore, it may be impossible for the identified model to estimate a quick change in the HR caused by external factors such as emotion and mental stress, which are not directly related to blood pressure. However, this problem may not be so important for the achievement of long survival with the TAH at the present time.

If the sampling interval can be modified appropriately by interpolation using a linear or a spline function, then Eq. 4 will be able to be theoretically applied to TAHs as an automatic control algorithm. To implement such a controller in an actual implantable TAH, however, the following problems must be solved.

1. In the same way as the 1/R control method, use of blood pressure as input information is not suitable for the implantable and durable TAH because pressure sensors are apt to drift and have low bioadaptability.
2. Since Eq. 4 holds only for normalized data with zero mean and unit variance, it is necessary to calculate the mean values and the standard deviations of input and output signals every time when these values seem to change.
3. In the case of the 1/R control method, it can be predicted that the AoP and RAP will, if they can, converge to the corresponding setting points. However, Eq. 4 does not have such setting points or reference values of blood pressures.

CONCLUSION

To develop a new control algorithm of the cardiac output of the TAH, a linear time series model representing heart rate variability as a function of the aortic pressure and right atrial pressure was proposed. The model was identified in an open-loop situation produced by the effectively total artificial heart implanted in a goat. Hence, it can be expected that the reliability and accuracy of the identified model were sufficiently high. Furthermore, the model could estimate the dynamic variation of the heart rate of the different goat as well as the response which was obtained due to a drastic change in the peripheral vascular resistance caused by a drug administration. As mentioned in the Discussion, however, a few serious problems are still to be solved before implementing the proposed model as a practical automatic controller for the TAH.

REFERENCES

1. Maslen EH, Bearnson GB, Bearnson GB, et al. Feedback control applications in artificial hearts. *IEEE Contr Syst* 1999;18:26–34.
2. Allen G, Murry K, Olsen D. Control of the artificial heart. *ASAIO J* 1996;42:932–7.
3. Kaufman R, Becker K, Nix C, Reul H, Rau G. Fuzzy control concept for a total artificial heart. *Artif Organs* 1995;19:355–61.
4. Tsach U, Geselowitz DB, Sinha A, Hsu HK. A novel output feedback pusher plate controller for the Penn State electric ventricular assist device. *J Dyn Syst* 1989;111:69–71.
5. Abe Y, Chinzei T, Mabuchi K, et al. Physiological control of a total artificial heart: conductance- and arterial pressure-based control. *Am J Physiol* 1998;84:868–76.
6. Yoshizawa M, Hashiya H, Takeda H, Yambe T, Nitta S. Simulation study on 1/R control strategy of the artificial heart. *Artificial Heart, 1993.* Switzerland: Harwood Academic Publishers, 1993;123–7.
7. Di Rienzo M, Mancia G, Parati G, Pedotti A, Zanchetti A. *Blood Pressure and Heart Rate Variability.* Amsterdam: IOS Press, 1993.
8. Sugimachi M, Imaizumi T, Sunagawa K, Hirooka Y, Todaka K, Takeshita A, Nakamura M. A new method to identify dynamic transduction properties of aortic baroreceptors. *Am J Physiol* 1990;258:887–95.
9. Kawada T, Sugimachi M, Sato T, et al. Closed-loop identification of carotid sinus baroreflex open-loop transfer characteristics in rabbits. *Am J Physiol* 1997;273:1024–31.
10. Goodwin GC, Sin KS. *Adaptive Filtering Prediction and Control.* New Jersey: Prentice Hall, 1998.
11. Nakamura M, Masuzawa T, Tatsumi E, et al. Control of total artificial heart using mixed venous oxygen saturation. *ASAIO J* 1999;45:460–5.

Functional Evaluation of an Artificial Anal Sphincter Using Shape Memory Alloys

YUN LUO,* TOSHIYUKI TAKAGI,* TAKESHI OKUYAMA,* SHINTARO AMAE,† MOTOSHI WADA,† KOTARO NISHI,† TAKAMICHI KAMIYAMA,† TOMOYUKI YAMBE,‡ AND HIDETOSHI MATSUKI§

This article describes an implantable artificial anal sphincter using shape memory alloys and its *in vivo* assessment in porcine models. The new design was developed as a low invasive prosthesis with a simple structure to solve the problem of severe fecal incontinence in patients with hypoplastic sphincters or without anal sphincters and especially for ostomates. The artificial anal sphincter consists of two shape memory alloy (SMA) plates as the main functional parts to perform two basic functions when the SMA artificial sphincter is fitted around intestines (*i.e.*, an occlusion at body temperature and an opening function on heating). Our previous assessments with short-term animal experiments revealed promising properties with the occlusion function of the device, although some complications, such as overpressure induced ischemia, heat burn, and infections, remained. This article addresses the concerns related to the practical use of the device, the power supplement to drive the actuator, and overheating protection of the device inside bodies. Results of chronic animal experiments of up to 4 weeks suggested great potential for the improved device. *ASAIO Journal* 2004; 50:338–343.

Incontinence, generally classified into urinary incontinence and fecal incontinence, has negative physical, psychologic, social, and economic effects on patients. Medical treatments, such as surgical reproduction of a neosphincter or electrical stimulation, have proved effective for selected patients. Artificial urinary sphincters have been developed and implanted in patients and have had a high success rate.[1,2] Meanwhile, little attention has been given to research on artificial anal sphincters. Prostheses with a structure similar to an inflatable circular cuff fitted around the anorectal bowel have been developed and studied in both animal experiments and clinical trials.[3–9] These implantations have improved incontinence, but they remain a controversial treatment, mainly because of reported mechanical failure and structures using a liquid drive mechanism. In addition, to be proportional to the dimension of the intestines, larger sizes of the cuff, balloon, and pump are required.

We proposed a novel artificial anal sphincter with a simple structure using shape memory alloys (SMAs). The purpose of this work was to reduce the number of parts of the device and to develop a compact design for a less invasive prosthesis.[10–12]

SMAs are functional materials with the unique characteristics of the shape memory effect (SME) and pseudo elasticity (PE). The features in the mechanical behavior of SMA materials, the high ratio of recovery force to weight, and large recoverable strains enable their applications for various compact actuators and sensors in industrial products, daily appliances, and medical applications.[13,14] The use of SME allows freedom in the design of medical actuators such as artificial muscles,[15] active catheters,[16] and SMA valves for urinary incontinence.[17] The commercialized artificial sphincter AMS-800 consists of three actuation required parts: an inflatable silicone cuff, a pressure regulating balloon, and a manual pump. The proposed artificial anal sphincter has only one deformable part (*i.e.*, the artificial sphincter itself), which is, therefore, expected to reduce the possibility of mechanical failure.

Our previous results from animal experiments on the preliminary evaluation of the SMA artificial anal sphincter showed promising properties for the occlusion of intestines.[11,12] However, postoperative complications and thermal burn were observed in tissues around the implanted device. The reasons for the problems have been attributed to the percutaneous lines connected to the external power supply and a lack of an overheating control in the device. In the current study, we made improvements (1) to decrease the potential for infection by incorporating a transcutaneous energy transmission (TET) system to realize complete implantation, thereby eliminating the potential for infection, and (2) to develop a thermal control inside bodies. Results of chronic animal experiments with the improved device are reported.

Materials and Methods

A typical SMA material with two way shape memory effect (TWSME), Ti51at%Ni, was adopted in this work. SMA plates were subjected to a solution treatment (850°C, 20 minutes) followed by an aging treatment (400°C, 100 hours) with restrained arc shapes. The transformation temperatures were measured by the differential scanning calorimetry (DSC) technique. At temperatures higher than body temperature, the material revealed only transformations between a rhombohedral phase (R-phase) and an austenite phase (A-phase). The start and finish temperatures are obtained by DSC measure-

From the *Institute of Fluid Science, Tohoku University, †Graduate School of Medicine, Tohoku University; ‡Institute of Development, Aging and Cancer, Tohoku University; and §Graduate School of Engineering, Tohoku University.

Submitted for consideration July 2003, accepted in revised form April 2004.

Correspondence: Yun Luo, Tohoku University Biomedical Engineering Research Organization, 2-1 Seiryo, Aoba-ku, Sendai 980-8575, Japan, e-mail: luo@tubero.tohoku.ac.jp

DOI: 10.1097/01.MAT.0000131819.07741.EF

ments: $A_s' = 47°C$, $A_f' = 52°C$ for A-phase and $M_s' = 49.5°C$, $M_f' = 44.5°C$ for R-phase.

A schematic drawing of the proposed artificial anal sphincter is shown in **Figure 1**. The actuator consists of two SMA plates jointed by hinges at their ends and foil type heaters attached on the SMA plates. Each SMA plate is 65 mm long, 15 mm wide, and 0.7 mm thick. Silicone pillows are placed on the surfaces of the SMA plates to prevent the pressure concentration on intestines that causes ischemia. Another function of the silicone pillows is for thermal insulation, because the highest temperature for the complete reverse transformation of the SMA might be higher than Af', although the maximum tolerable temperature for tissues of living bodies is approximately 42°C. The artificial sphincter can be fitted around intestines and act with an occlusive force on the intestines at body temperature. On heating, the reverse R-phase transformation occurs in the SMA plates, accompanied by the shape changes from a flat shape to an arc shape. The shape change results in a lumen between two SMA plates, which allows bowel movement. After switching off the electrical power for heating, the SMA plates recover to their initial shapes on natural cooling, closing the intestines again. A prototype of the developed artificial sphincter is shown in **Figure 2**. It is 80 mm long, 15 mm wide, and 20 mm high. The SMA material in its rhombohedral phase, which exists at body temperature, has a lower Young's modulus than that in its austenite phase, and is easy to deform mechanically. This characteristic enables another function for healing the intestines after the implantation. If we deform the SMA ribbons to arc shapes to have a lumen in the artificial sphincter, this open state would be maintained as long as the SMA artificial sphincter is deactivated. After several days, thermal activation or deactivation can be used to open or close the intestines.

The power to heat the SMA plates can be provided percutaneously by a DC/AC external power supply, but in our previous animal experiments, it was difficult to avoid infection along the electrical lines.[11] The TET system, a technology developed for the power supply of artificial hearts,[18] was then adopted for our artificial anal sphincter. Integrating the TET systems into the SMA actuator can facilitate the complete implantation of an artificial anal sphincter and can eliminate the potential for infection.

The basic design of the device has two elements implanted inside the body: an SMA based artificial sphincter and a secondary coil. Although the former has a comparable dimension to the silicone cuff in the AMS-800, the latter is disklike and drastically reduces the volume of the implant. This promotes the new device as a low invasive prosthesis. In addition, the simple mechanism of the driving principle of the device is expected to enhance its reliability and durability.

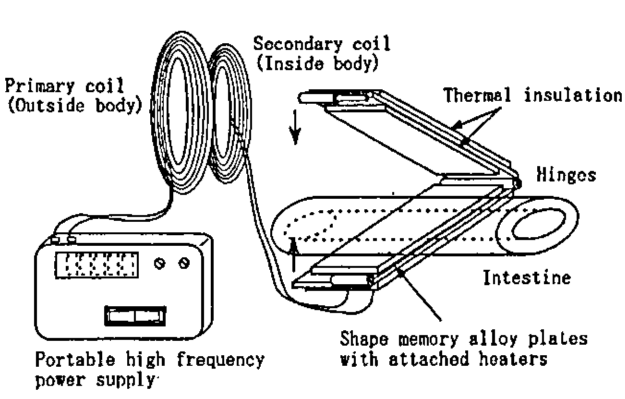

Figure 1. Schematic drawing of the proposed artificial anal sphincter using shape memory alloy.

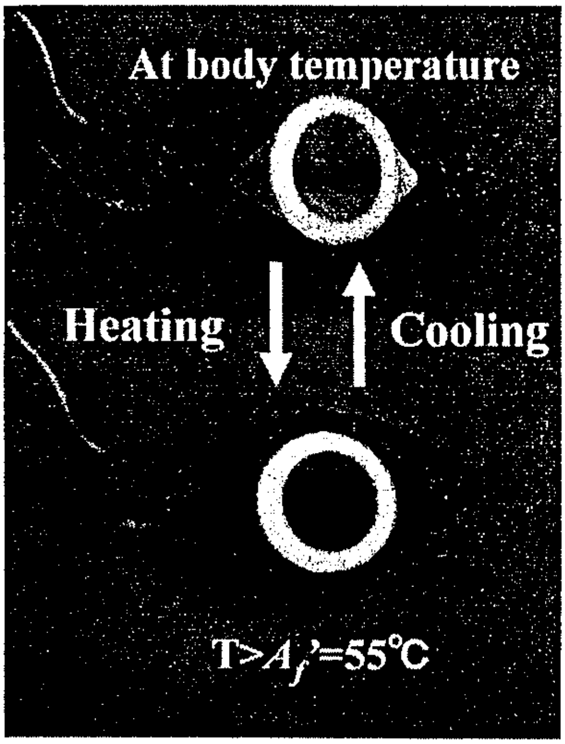

Figure 2. A prototype of the proposed artificial anal sphincter clipping an artificial intestine (upper) and deformed for releasing function (bottom). T, temperature; A_f', finish temperature of reverse transformation.

Results and Discussion

Deformation Under Thermal Cycles

The thermomechanical properties were investigated to determine the maximum obtainable gap between the middle points of two deformed SMA plates large enough to allow a bowel movement. The gap was indirectly evaluated by measuring the strain on the surfaces of the SMA plates. The temperature dependence of the strain is presented in **Figure 3**. As seen in **Figure 3**, on heating, the strain increases slightly from the 43°C because of the local transformation and exhibits a sharp rise from 47°C, corresponding to the start temperature of the reverse transformation, followed by saturating at a maximum value of strain. On cooling until the temperature decreases to the start temperature of the R-phase transformation, the strain remains at the maximum value. The time for this temperature drop allows for the bowel movement. In addition, complete shape recovery was obtained when the temperature dropped to the initial value. The maximum strain ϵ has the relation with the curvature ρ for a specific thickness t, $\epsilon = t/2\rho$. Therefore, for the maximum strain of 1.2% and thickness of 0.7 mm, the curvature is calculated to be approximately 30 mm.

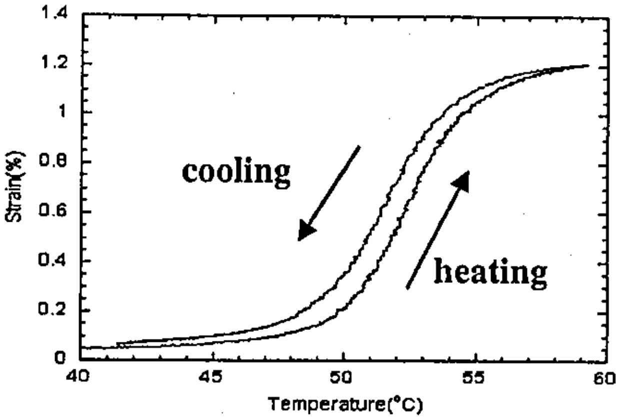

Figure 3. Transformation accompanied strain changes in a Ti51 at %Ni plate underwent a aging treatment with a restrained shape.

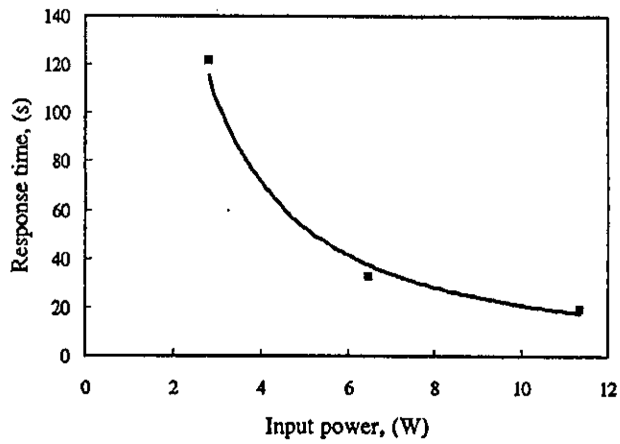

Figure 4. Input power dependences of the response time in an *in vivo* experiment.

The initial strain of the SMA plates is generated by the silicone pillows attached on their inner surfaces. The maximum strain leads to a lumen between two SMA plates of around 30 mm. The practical lumen for opening the intestines should subtract the thickness of silicone pillows 10 mm (5 mm for each one). This lumen was proved adequate for providing appropriate pressure on intestines in our animal experiments. For clinical trials in the future, this lumen should be set to fit the dimension of the intestines of individual patients through a careful design, taking into account the mechanical interaction between the SMA ribbons, silicone pillows, and natural intestines.

Transient Thermal Responses of the Artificial Sphincter

In our previous study, *in vitro* investigations were conducted on the time response of SMAs and the temperature dependent occlusive properties.[11] At room temperature, the artificial anal sphincter exhibited a good occlusive function against hydrostatic pressures of up to 75 mm Hg, although the mean inner pressure of intestines is estimated to be around 50 mm Hg for human bodies. *In vivo* experiments were performed in the current work to investigate the relationship between the input electrical power and response time. Preliminary tests were carried out, heating the SMA plates from the body temperature to around 60°C by a DC power supply. The transient temperature of the SMA plates was measured by a thermocouple sandwiched between SMA plates and thermal insulations. The input voltage of the power supply was set to 8 V, 12 V, and 16 V for three cases. Because the electrical resistance of the heaters is 22 Ohm, the power for each case becomes 2.9 W, 6.5 W, and 11.5 W. As shown in **Figure 4**, the time responses were 122 seconds, 33 seconds, and 19 seconds for corresponding cases. To obtain a shorter response time, more power is required. The temperatures on the contacting surfaces of the silicone pillows with intestines (inner surface) and the surrounding tissues (outer surface) were measured by thermocouples for confirmation purposes because surface temperatures of the device should be maintained lower than the maximum tolerance value of tissues, 42°C. **Figure 5** shows the results of a representative case with electrical power of 6.48 W (0.54 A, 12 V) and 33 seconds for heating. The power was applied to heat the SMA plates to 60°C and then switched off. The response time was found to be around a half minute. Slight temperature rises were observed on the inner and outer surfaces, but the highest temperatures were lower than 40°C. The peak of the temperature rises on surfaces appeared with a time delay compared with that of SMA plates because of transient heat conduction. The difference in their responses is attributed to the difference in the thickness of thermal insulations: 3 mm for the outer surface and 4 mm for the inner.

Transcutaneous Energy Transmission System

To power implantable devices, TET systems are most suitable for achieving complete implantation, thereby reducing the potential for postoperative infections that are usually difficult to avoid in applications with percutaneous power supply leads. Ventricular assist devices are well known applications of the TET system.[19-21] A typical TET system setup consists of an AC power supply connected with a primary coil providing an alternating field and a secondary coil in which the AC current can be induced and coupled with a load.

For medical applications of TET systems, the thermal effect of

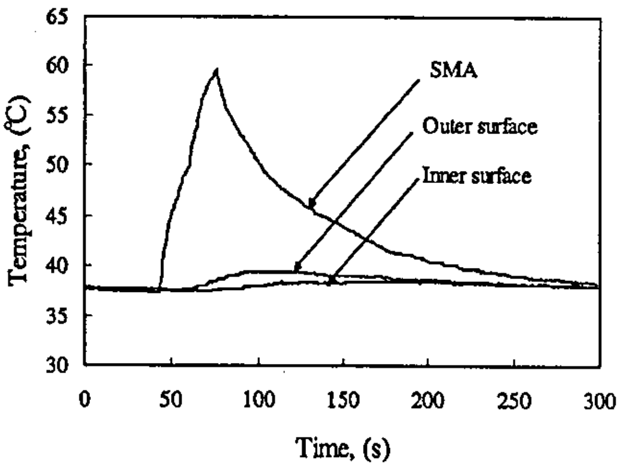

Figure 5. Thermal response of the artificial anal sphincter in an *in vivo* experiment. SMA, shape memory alloy.

the implanted secondary coil on the contacting tissues should be taken into account. Enhancement of energy transfer efficiency is also a common concern in this technology. The thermal effect of the coils on the contacting tissues should be lower than 42°C by reducing the electrical resistance of the coils.[20] However, the optimization of the profile of coils to obtain higher energy transfer efficiency depends on many factors, such as the distance between the primary and secondary coils (defined as coil separation) and the materials of the coil core. A detailed discussion on these topics is beyond the focus of this article. Here we investigated the possibility of power transmission to drive the artificial anal sphincter with adequate coil separations for practical uses. The system, with its block diagram illustrated in **Figure 6**, consists of a high frequency power supply connected to the primary coil L1, a secondary coil L2 connected to the SMA artificial anal sphincter, and spacers with corresponding thickness sandwiched between two disc shaped coils. The coils were made from a twisted bunch of 100 thin copper wires, each with diameter of 0.1 mm. The primary coil has 10 turns of the bunch and has outer and inner diameters of 60 mm and 30 mm. The secondary coil has 8 turns, and its outer and inner diameters are 40 mm and 20 mm. Preliminary experiments have been demonstrated *in vitro* for three cases with the coil separations being 5 mm, 10 mm, and 15 mm. The power with a frequency of 100 kHz was applied in the primary coil with 15 V, 18 V, and 22 V for each case. The power factors depend on the configuration of the experimental setup (here, mainly the coil separation); therefore, the values of power obtained in the coils increase with the decrease of coil separations, and the obtained efficiency exhibits a similar tendency as that seen in **Figure 7**. In a case with a coil separation of 15 mm, the energy transfer efficiency is 56%, and it increases to 70% for a coil separation of 10 mm and to 88% for 5 mm. For a case with a coil separation of 10 mm, which is comparable with cases in practice and power of 10 W, the response time is shorter than half a minute.

In summary, although in animal experiments the secondary coil is implanted under skin with a distance ranging from 5–8 mm from the primary coil, the developed TET system exhibits a capability in energy transfer to the artificial anal sphincter with the coil separations over a range of 5–15 mm with satisfactory responses.

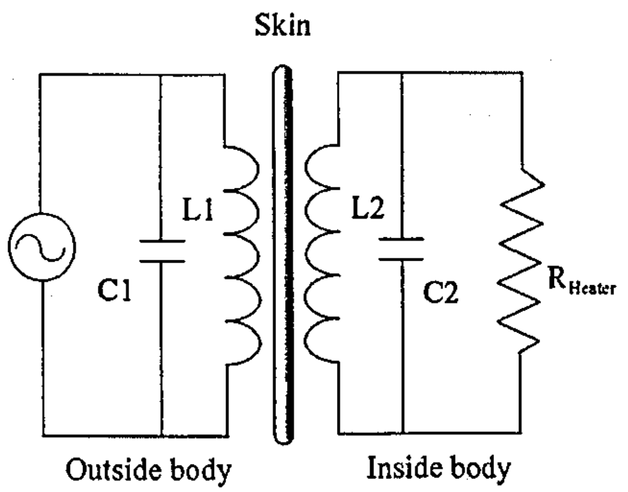

Figure 6. Schematic drawing of a transcutaneous energy transmission system for driving the artificial anal sphincter (indicated by R_{Heater}). L1, primary coil; L2, secondary coil; C1, primary capacitor; C2, secondary capacitor.

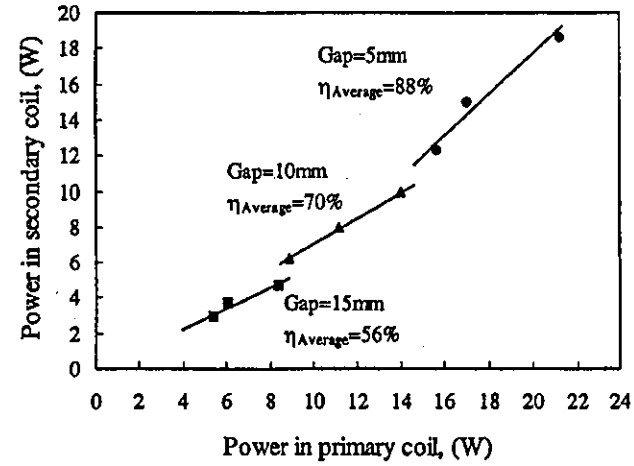

Figure 7. Gap dependency of energy transmission efficiencies with different coil gaps.

Thermal Control

As previously mentioned, a simple switch off control of the applied power can prevent the SMA plates from overheating after a complete deformation. With the maximum temperature being controlled, the temperatures on the contacting surfaces of the silicone pillows with intestines (inner surface) and the surrounding tissues (outer surface) were controlled successfully to be lower than the maximum tolerance value of tissues, 42°C. Because there is no deformation in the temperature range from Af to the start temperature of R-phase transformation Ms, the deformed shape could be maintained for a short period as long as the temperatures were higher than Ms. However, the short period, usually less than 1 minute, was not long enough for the bowel movement. This concern motivated us to develop an approach to control the temperature of SMA plates at around Af, automatically, to elongate the open time without overheating the surrounding tissues.

For this purpose, we introduced a temperature sensitive reed switch (normally closed) into the electrical circuit of the inside part of the device. The switch consists of two permanent magnets and a thermal sensitive ferrite tube, forming a magnetic circuit. A ferromagnetic contacting pair closes normally under a balance between an elastic force and a magnetic force induced by the magnetic field. Heating the ferrite tube reduced its magnetization, and as the temperature exceeded its Curie point, the magnetization dropped to zero, leading to the opening of the magnetic circuit. Without the magnetic force, the contacting pair was opened by the elastic force. It is expected that such a switch will be used to perform on–off control of power applied in the artificial sphincter. The best way is to use a switch directly attached on the SMA to control its temperatures. However, the size of commercially those available inhibits such a design. In this work, an additional heater was used to heat the reed switch. The switch was electrically connected with the SMA sphincter in series. A schematic

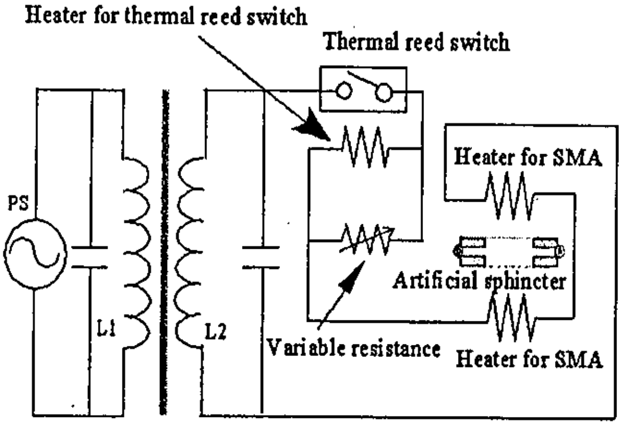

Figure 8. Schematic drawing of the electrical circuit of the proposed system. SMA, shape memory alloy.

drawing of the proposed set is illustrated in **Figure 8**. A thermal sensitive reed switch with a 55°C operating temperature was adopted in the control circuit. To ensure the temperature of the SMA plates could be controlled at A_s', a variable resistor, connected with the additional heater in parallel, was used to bypass the current in the reed switch. Experiments for the confirmation of the proposed approach were conducted. To confirm the robustness of the control scheme, a demonstration of the temperature responses under a variation of applied power was conducted, with a fixed value of the variable resistor. Results of the cases with applied voltage of 15 V and 25 V are shown in **Figure 9**. In each case, the temperature of the reed switch was successfully controlled with an on–off switching at approximately the operating temperature of 55°C. Meanwhile, the average temperature of the SMA plates was successfully controlled at approximately 60°C. This suggests that once the overheating of the SMA plates is controlled, the surface temperatures of the artificial sphincter can be controlled below a certain value by increasing the thickness of the thermal insulation materials. An *in vivo* example is shown in **Figure 10**; the temperature of SMA plates was successfully controlled within a range from 58°C to 65°C, which ensures

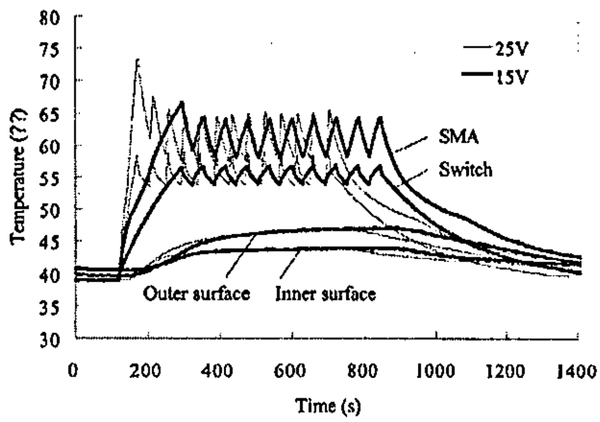

Figure 9. Temperature responses of the shape memory alloy (SMA) plates, the reed switch, and surfaces of the artificial sphincter with applied voltages of 25 V and 15 V.

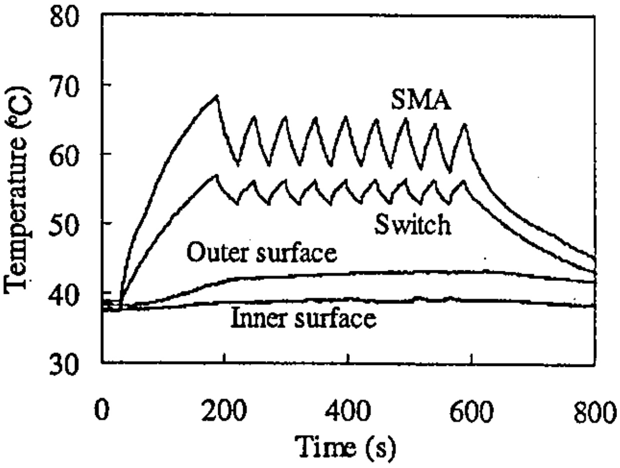

Figure 10. Thermal responses of the artificial sphincter inside the body but with corrected parameters. SMA, shape memory alloy.

the open function of the artificial sphincter. During the operating period of 10 minutes, the surface temperatures did not exceed 43°C. The inner surface, defined as the contact area with the intestines, was found to be much lower than the outer surface because of the difference in the thickness of the thermal insulation. A further reduction of the surface temperatures of the artificial sphincter can be realized easily by increasing the thickness of insulation materials covering the SMA plates.

Animal Experiments

A series of animal experiments, including acute and chronic experiments, were performed on porcine models with weights ranging from 15 kg to 20 kg. All animal experiments were performed with permission issued by the Committee on Animal Experiments in Tohoku University. In our acute experiments, basic functions of the artificial sphincter (*e.g.*, the open occlusion function, the resting anal pressure after implantation, and the thermal behavior of the device) were investigated. Chronic experiments were conducted in two stage operations: a colostomy on the abdomen through the oblique muscles, followed by implantation of the artificial anal sphincter. The colostomy before the implantation of the device is a procedure conducted only to create a situation of complete fecal incontinence in animal models rather than a necessary preoperation to implant the device. For the practical use of the device, the colostomy would, of course, not be required. So, even though this protocol is very invasive, the device itself should not be considered invasive because of the colostomy. In a previous paper, we reported preliminary results on two animal models.[11] Although the occlusion function as a sphincter was completely confirmed with a maximum pressure of 55 mm Hg, severe postoperative complications were found. Problems observed in these experiments were then improved with the new design. For example, the incorporation of the TET system is expected to eliminate postoperative infections and the overheating protector to reduce the thermal impact on surrounding tissues.

With the improved devices, we performed three chronic animal experiments. Two lasted 2 weeks, and one lasted 4 weeks. The occlusion pressures were measured after each implantation. Average values were found ranging from 40 mm Hg to 50 mm Hg. In the former two experiments, without overheating protection, activation of the device was performed by a simple on–off operation of the power supply. Although at the beginning, fecal continence was regularly observed, constipation was found several days after operation. A possible reason was considered to be the relatively short open time of around 1 minute, which may be not enough for complete evacuation. This problem was solved in the latest experiment. By incorporating the thermal controller into the device, the open time was lengthened to 10 minutes. During the 4 weeks of the experiment, fecal movements were regularly observed when the artificial anal sphincter was activated, and the evacuated feces was confirmed as being normal by comparing with that of controls. At autopsy, postoperative infection was found in a pocket containing the thermal controller, perhaps because of some failure of the silicone coating. Slight burns were found on the surfaces of tissues contacting with the secondary coil and the side face of the artificial sphincter, where the thermal insulations are relatively thin. Nevertheless, neither ischemic anomaly nor heat burn was found in tissues that underwent occlusion pressure most of the time, suggesting the good functionality of the developed artificial anal sphincter.

Conclusion

In summary, an SMA artificial anal sphincter actuated by a TET system has been developed for complete implantation. The use of Ti51 at %Ni, which exhibits TWSME, enables a compact design with simple structure. Fundamental thermomechanical behaviors of the SMA actuator have been investigated in both *in vivo* and *in vitro* experiments. Satisfactory occlusion and release functions of the artificial sphincter were confirmed. Thermal control using a thermal sensitive reed switch was incorporated into the device to prevent the temperature of the SMA plates from overheating. This approach proved effective, allowing a long enough open time of the artificial sphincter for evacuation, and the overheating protection was found to be robust against possible changes in the values of the applied power. The developed SMA artificial sphincter has been implanted in animal models for chronic experiments of up to 4 weeks and has exhibited good performance in maintaining fecal continence.

Results obtained in the current work suggest the possibility of the SMA artificial anal sphincter as a new solution for severe fecal incontinence. However, the assessment of its biocompatibility requires longer animal experiments. Concerning the biocompatibility of materials used in the current work, the TiNi SMAs may give rise to a problem of the possible dissolution of Ni, which is considered toxic. It was reported that an adequate surface treatment such as laser surface melting could dramatically increase the corrosion resistance of the alloys.[22] Moreover, coating the TiNi alloy with polyurethanes followed by 2-methacryloyloxy ethyl phosphorylcholine (MPC) polymers[23] that have been proven to have good biocompatibility should be effective in resisting the corrosion of Ni and making the device biocompatible. In our future work, long-term animal experiments with the SMA artificial anal sphincter implanted will be repeated to confirm the biocompatibility of the device.

Acknowledgement

This research was supported by the Industrial Technology Research Grant Program in 2000 (00A45027) from the New Energy and Industrial Technology Development Organization (NEDO) of Japan.

References

1. Hajivassiliou CA: A review of the complications and results of implantation of the AMS artificial urinary sphincter. *Eur Urol* 35: 36–44, 1999.
2. Petrou SP, Elliott DS, Barrett DM: Artificial urethral sphincter for incontinence. *Urology* 56: 353–359, 2000.
3. Christiansen J, Lorentzen M: Implantation of artificial sphincter for anal incontinence. *Lancet* 1: 244–245, 1987.
4. Lehur PA, Michot F, Denis P, *et al:* Results of artificial sphincter in severe anal incontinence. Report of 14 consecutive implantations. *Dis Colon Rectum* 39: 1352–1355, 1996.
5. Hajivassiliou CA, Carter KB, Finlay IG: Assessment of a novel implantable artificial anal sphincter. *Dis Colon Rectum* 40: 711–717, 1997.
6. Vaizey CJ, Kamm MA, Gold DM, Bartram CI, Halligan S, Nicholls RJ: Clinical, physiological, and radiological study of a new purpose-designed artificial bowel sphincter. *Lancet* 352: 105–109, 1998.
7. Lehur PA, Roig JV, Duinslaeger M: Artificial anal sphincter: Prospective clinical and manometric evaluation. *Dis Colon Rectum* 43: 1100–1106, 2000.
8. Lehur PA, Frank Z, Michel N, Pascal G, Stanislas BV: Comparison of quality of life and anorectal function after artificial sphincter implantation. *Dis Colon Rectum* 45: 508–513, 2002.
9. Hajivassiliou CA, Carter KB, Finlay IG: Biomechanical evaluation of an artificial anal sphincter prosthesis. *J Med Eng Technol* 21(3–4): 89–95, 1997.
10. Takagi T, Luo Y, Hara S, *et al:* An artificial sphincter using shape memory alloy actuators. *Journal of Advanced Science* 12: 337–342, 2000.
11. Amae S, Wada M, Luo Y, *et al.* Development of an implantable artificial anal sphincter by the use of the shape memory alloy (SMA). *ASAIO J* 47: 346–350, 2001.
12. Luo Y, Takagi T, Amae S, *et al:* An SMA artificial anal sphincter actuated by transcutaneous energy transmission systems. *Materials Transactions* 43: 1052–1056, 2002.
13. Kapgan M, Melton KN: Shape memory alloy tube und pipe couplings in Duerig TW, Melton KN, Stockel D, Wayman CM (eds.), *Engineering Aspects of Shape Memory Alloys.* London; Boston: Butterworth-Heinemann, 1990, pp. 137–148.
14. Ohkata I, Suzuki Y. The design and shape memory alloy actuators and their applications in Otuska K, Wayman CM (eds.), *Shape Memory Materials.* Cambridge: Cambridge University Press, 1998, pp. 240–266.
15. Maruyama S, Kawase M, Sakai S, *et al:* Proposal of thermoelectric actuator and development of active catheter. *JSME International Journal,* Series B 43(4): 712–718, 2000.
16. Park K, Lim G, Sugihara M, Minami K, Esashi M: Future of active catheters. *Sensors and Actuators A: Physical* 56(1–2): 113–121, 1996.
17. Chonan S, Jian ZW, Tani J, *et al:* Development of an artificial urethral valve using SMA actuators. *Smart Materials and Structures* 6: 410–414, 1997.
18. Mitamura Y, Hirano A, Okamoto E, Mikami T: Development of transcutaneous energy transmission system, in Akutsu T (ed.), *Artificial Heat-2.* Tokyo, Japan: Springer, 1988, pp. 265–270.
19. Weiss WJ, Rosenberg GR, Snyder AJ, Pae WE, Richenbacher WE, Pierce WS: *In vivo* performance of a transcutaneous energy transmission system with the Penn State motor driven ventricular assist device. *ASAIO Transactions* XXXV: 284–288, 1989.
20. Mussivand T, Miller JA, Santerre PJ, *et al:* Transcutaneous energy transfer system performance evaluation. *Artificial Organs* 17: 940–947, 1993.
21. Mussivand T, Holmes KS, Hum A, Keon WJ: Transcutaneous energy transfer with voltage regulation for rotary blood pumps. *Artif Organs* 20: 621–624, 1996.
22. Villermaux F, Tabrizian M, Yahia L'H, Meunier M, Piron DL: Excimer laser treatment of NiTi shape memory alloy biomaterials. *Applied Surface Science* 109/110: 62–66, 1997.
23. Ishihara K: Bioinspired phospholipid polymer biomaterials for making high performance artificial organs. *Science and Technology of Advanced Materials* 1: 131–138, 2000.

J. Micromech. Microeng. 15 (2005) 71–75 doi:10.1088/0960-1317/15/1/011

Ultra-miniature fiber-optic pressure sensor using white light interferometry

Kentaro Totsu[1], Yoichi Haga[2] and Masayoshi Esashi[3]

[1] Graduate School of Engineering, Tohoku University, 01 Aza-Aoba, Aramaki, Aoba-ku, Sendai 980-8579, Japan
[2] Tohoku University Biomedical Engineering Research Organization (TUBERO), 01 Aza-Aoba, Aramaki, Aoba-ku, Sendai 980-8579, Japan
[3] New Industry Creation Hatchery Center (NICHe), Tohoku University, 04 Aza-Aoba, Aramaki, Aoba-ku, Sendai 980-8579, Japan

E-mail: totsu@mems.mech.tohoku.ac.jp

Received 11 May 2004, in final form 2 August 2004
Published 8 October 2004
Online at stacks.iop.org/JMM/15/71

Abstract
We have developed a fiber-optic Fabry–Perot interferometric pressure sensor of 125 μm in diameter and a detection system for medical use. A Fabry–Perot cavity is formed at an optical fiber end. A deformation of the diaphragm of the Fabry–Perot cavity induced by pressure varies the cavity length. White light interferometry is used to avoid error and noise caused by bending of the optical fiber and fluctuation of the light source. The reflection light of the sensor cavity is detected by a commercial high-speed spectrometer. A pressure change has been detected by using the developed sensor system. Animal experiments using a goat have been carried out and dynamic pressure changes in the internal pressure of heart and aorta have been successfully monitored.

(Some figures in this article are in colour only in the electronic version)

1. Introduction

In medical diagnosis and treatment, pressure measurement is essential for monitoring the condition of a human body. Furthermore, the spread of minimally invasive therapy (e.g., percutaneous coronary intervention) requires monitoring local pressure in a very narrow space. To meet the demands, a miniaturized pressure sensor has been developed [1–6]. The pressure sensors utilize piezoresistive and optical detection using optical fibers. In particular, fiber-optic pressure sensors have the advantages of not only high potential of miniaturization but also applicability to use in such electromagnetically harsh environments as in an operating room in a hospital. Although small fiber-optic sensors have been commercialized, still it is difficult to meet the demands of the size and the shape. To realize the smallest and finest shape, a pressure sensor of 125 μm in diameter was developed in our research [7, 8]. The Fabry–Perot interferometric sensor the cavity length of which was changed by pressure was formed at the tip of the optical fiber. However, though the pressure sensor was small enough to install in interventional tools (e.g., catheter, guide wire), bending of the optical fiber and fluctuation of the laser diode used as the light source affected the sensor output. To reduce the effects of bending and fluctuation on the sensor output, a real-time measurement system which used spectrum modulation shifted by the distance change of the mirrors of the sensor cavity has been utilized. In this paper, we describe an ultra-miniature fiber-optic pressure sensor and a detection system for *in vivo* blood pressure monitoring.

2. Sensor system

The structure of the fiber-optic pressure sensor is shown in figure 1. The sensing element of 120 μm in diameter is composed of a thin silicon dioxide diaphragm with a mesa, an aluminum mirror on the mesa and a spacer fabricated by micromachining. It is bonded to the end of a multimode optical fiber. The outer diameter and the core diameter of the optical fiber are 125 μm and 50 μm, respectively. A chromium half-mirror is formed at the fiber end. A ring-shaped spacer made of polyimide (2 μm thick) is formed. The aluminum mirror and the chromium mirror spaced by the cavity constitute a

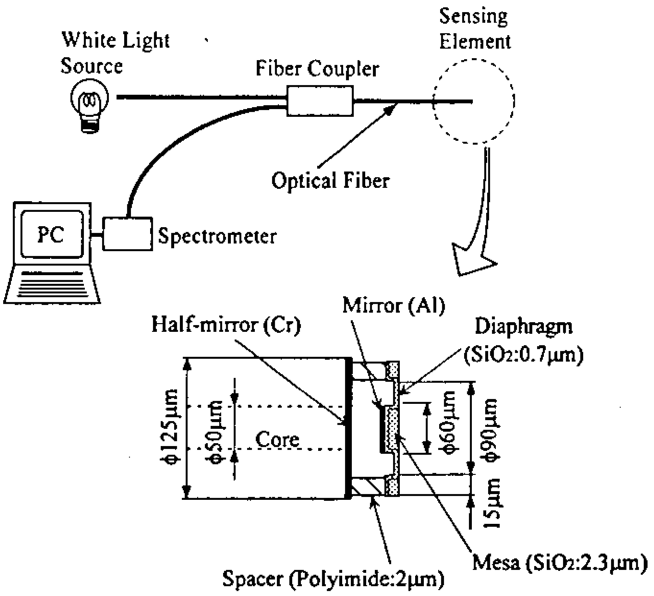

Figure 1. Schematic of sensor system.

Fabry–Perot interferometer (FPI) at the fiber end. The initial cavity length of the FPI is about 2 μm.

The deformation of the diaphragm induced by the pressure varies the cavity length. White light interferometry is utilized to detect the deformation of the diaphragm [9]. Low-coherence light from a white light source passes through the optical fiber to the sensor, and then the light is modulated at the FPI of the sensor. The light reflected by the sensor passes through the optical fiber again and is detected by a spectrometer. The cavity length d corresponding to applied pressure is determined by measuring the spectrum of the reflection light of the sensor. The cavity length d can be obtained by using

$$d = \frac{\lambda_1 \lambda_2}{2n(\lambda_2 - \lambda_1)}$$

where n represents the refractive index of the material of the sensor cavity, λ_1 and λ_2 represent adjacent peaks in the reflection spectrum [10].

Since the bending loss of the optical fibers and the fluctuation of the light source do not change the peak wavelengths of the spectrum but vary the total intensity of detected light, white light interferometry can reduce the influence of the bending loss and fluctuations on the output of the sensor system [11–14].

3. Sensor fabrication

The sensing element with a silicon column is batch fabricated on a silicon wafer by micromachining and is bonded to the half-mirror-coated optical fiber end utilizing patterned polyimide layer by thermocompression as shown in figure 2. After the bonding, unnecessary silicon column parts are removed by xenon difluoride (XeF_2) etching [8].

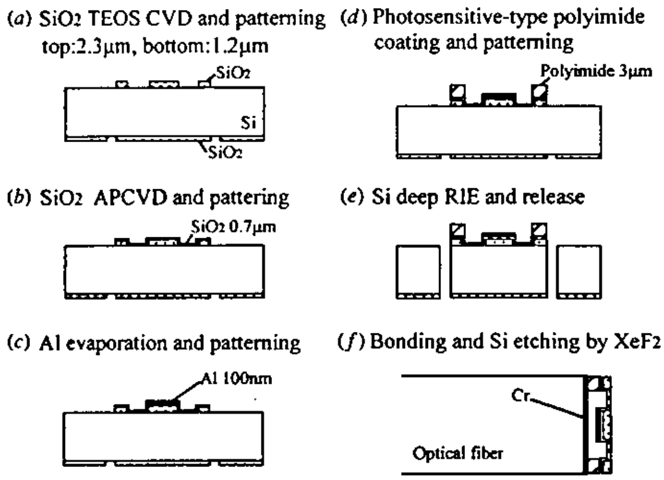

Figure 2. Schematic of the process for micromachined sensor structure.

Figure 3. Photograph of fabricated silicon columns with sensing element.

(a) Silicon dioxide film is deposited on both sides of a 200 μm thick silicon wafer by plasma-enhanced chemical vapor deposition (PECVD) using a tetraethoxysilane (TEOS) source. The film thickness of the top side is 2.3 μm and that of the bottom side is 1.2 μm. These silicon dioxide films are patterned for the mesa (top side) which keeps the aluminum reflecting mirror flat and the etching mask (bottom side) used in the later silicon deep reactive ion etching (deep RIE) process (e).

(b) Silicon dioxide film (0.7 μm thick) is deposited by atmospheric pressure chemical vapor deposition (APCVD) and is patterned.

(c) Aluminum is evaporated in vacuum and is patterned by a lift-off process for the reflecting mirror.

(d) Photosensitive-type polyimide (3 μm thick) is spin-coated and is patterned for the bonding layer and the spacer for the sensor interferometer.

(e) The silicon wafer is etched by silicon deep RIE. Then the sensing elements are released from the wafer.

(f) A thin chromium transparent layer as a half-mirror is coated on the end of the optical fiber in advance and the sensing element with the silicon column is bonded to the fiber end. Then the silicon part supporting the sensing element is etched by XeF_2.

As the result of the fabrication process, many sensing elements with silicon column are batch fabricated as shown in figure 3. The diameter of the silicon column is 120 μm, and the length is 200 μm, which is almost equal to the wafer thickness. Approximately 100 000 pieces of sensor elements

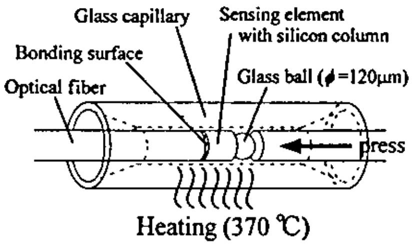

Figure 4. Schematic of the bonding process of sensing element to optical fiber end.

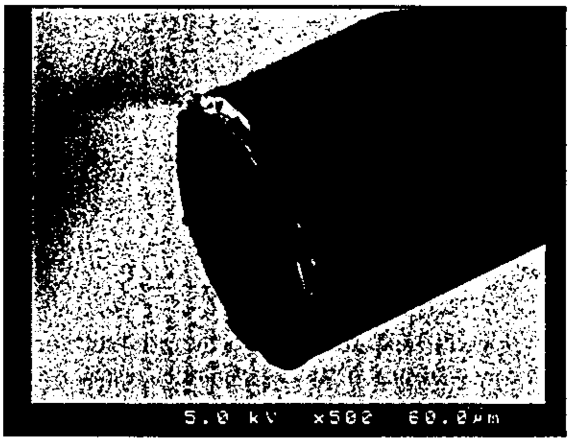

Figure 5. SEM photograph of fabricated pressure sensor of 125 μm in diameter.

can be obtained from a 4 inch silicon wafer. As this miniature pressure sensor can be produced at relatively low cost, it is suitable for disposable use, which is efficient for use in blood vessels.

A cleaved fiber end is coated with chromium by evaporation to make the half-mirror. The thickness of the chromium layer is about 10 nm. A metal half-mirror is optically neutral, which means that the reflectance and the transmittance do not depend on wavelength for a wide range. Therefore, it is effective for white light interferometry to achieve a linear sensor output.

The process of bonding the sensing element with silicon column to the half-mirror-coated optical fiber end is carried out in a glass micro capillary as a guide as shown in figure 4. The silicon column keeps the sensing element parallel to the fiber end in the glass capillary. The inner diameter of the capillary is 127 μm. The sensing element with silicon column and a micro glass ball of 120 μm in diameter are inserted into the capillary. The half-mirror-coated optical fiber is inserted into the capillary so as to face the sensing element. The other optical fiber is inserted from the other side and presses the polyimide layer of the sensing element on the fiber end. After confirming that the spectrum of the reflection light of the sensor is clearly observed, the capillary is heated stepwise up to 370 °C to bond the sensing element with silicon column to the fiber end.

After the bonding process, the silicon column is fully removed by XeF_2 etching. Figure 5 shows an SEM photograph of the completed sensor. The ultra-miniature sensing element at the fiber end can be observed.

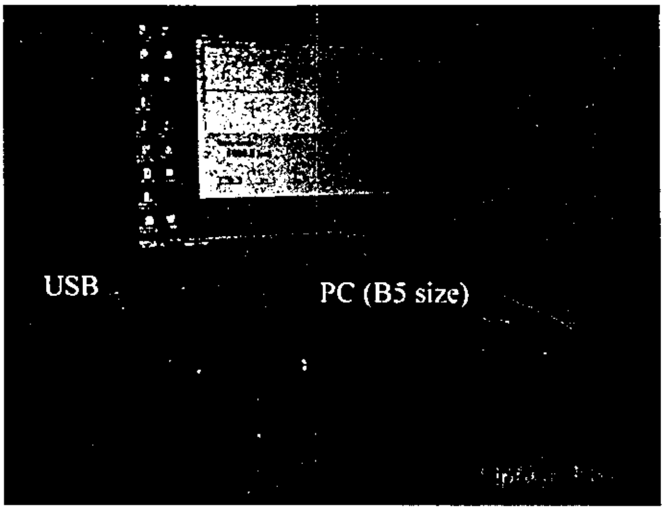

Figure 6. Photograph of developed fiber-optic pressure sensor system.

4. Experimental setup

The experimental setup of the developed sensor system is the same as shown in figure 1. The white light generated by a halogen lamp (OCEAN OPTICS, LS-1) reaches the sensor cavity and is modulated. The spectrum of the reflection light of the sensor cavity is detected by a miniature fiber-optic high-speed spectrometer (OCEAN OPTICS, USB2000). The captured spectrum data are transferred to a personal computer (PC) via a USB connection and are used to obtain the cavity length of the sensor. The cavity length is converted to a pressure value and then the pressure value is continuously displayed on the monitor of the PC. The sampling rate is about 70 Hz and it mainly depends on sampling at the spectrometer, the data transfer from the spectrometer to the PC. The developed sensor system is shown in figure 6. The white light source, the fiber coupler and the spectrometer are built into the box under the B5-size PC.

5. Experimental results

5.1. Measurement in a pressure-controlled chamber

The fabricated fiber-optic pressure sensor was tested in a chamber connected to a pressure controller (NAGANO KEIKI, PC10). Figure 7 shows the reflection spectrum of the sensor for different pressures. Spectrum modulation was obtained and the peak shifts were clearly monitored. The measured cavity length using the spectrum data, as a function of applied pressure, is shown in figure 8. A least-squares fit of these data yields the sensitivity of -0.25 nm mmHg^{-1} with the correlation coefficient having a value of 0.9993 and the resolution of 4 mmHg for pressures ranging from -100 to 400 mmHg. Averaging of the acquired cavity lengths calculated using more than one pair of peaks and interpolation between sampling data of pixels of the spectrometer contribute high resolution and low noise measurement. The resolution can be improved by noise reduction of the spectrometer or increasing the displacement of the diaphragm.

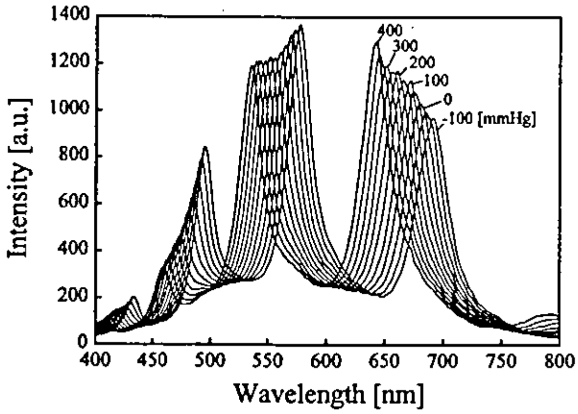

Figure 7. Reflection spectrum of developed pressure sensor for different applied pressures.

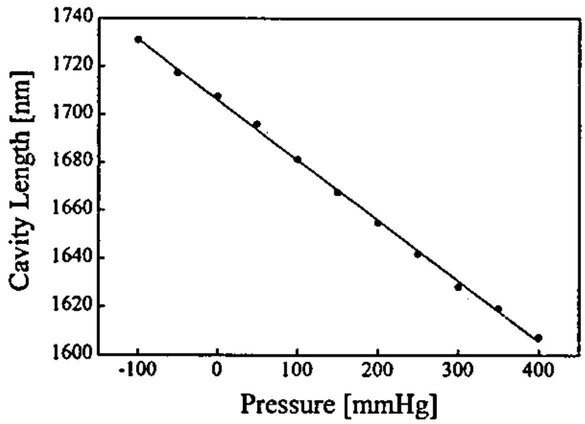

Figure 8. Detected sensor cavity length as a function of pressure.

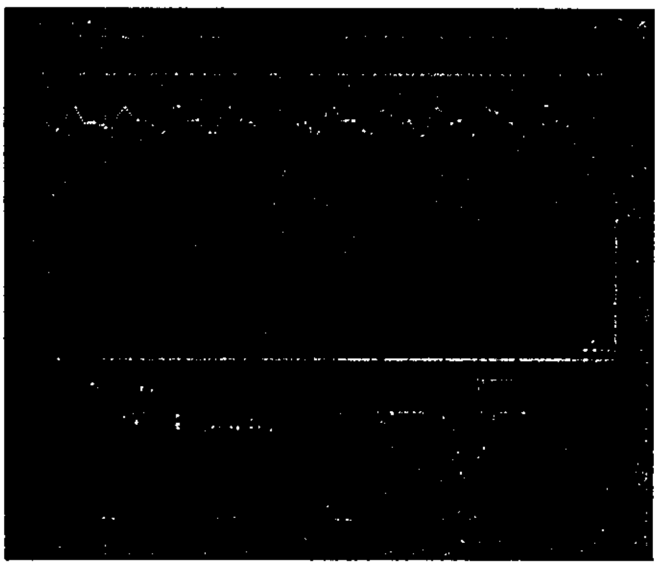

Figure 9. Continuous display of blood pressure in the aorta of a goat.

5.2. *Experiments on animals*

Experiments on animals have been carried out. The developed sensor system was applied for monitoring blood pressure in the left ventricle, left atrium, right atrium and aorta of a goat. The ultra-miniature fiber-optic pressure sensor was set in an injection needle of which the outer diameter was about 0.6 mm. Figures 9 and 10 show one of the results of monitoring the blood pressure in aorta and left ventricle, respectively. The pressures were successfully monitored and the waveforms of the dynamic pressure change were clearly observed.

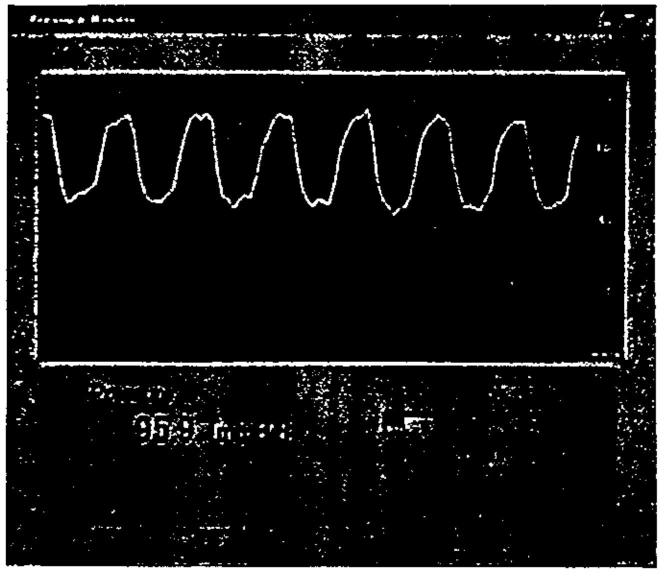

Figure 10. Continuous display of blood pressure in the left ventricle of a goat.

6. Discussion

Owing to the low sampling frequency of the sensor system, disturbed waveforms of pressure have been observed. The sampling frequency depends on the data transfer rate from the spectrometer to the PC. A microcontroller-based spectrometer is suitable for increasing the data transfer rate for realizing higher sampling frequency utilizing parallel data processing.

During the pressure measurements, the influence of temperature change on the sensor output was observed. Specifically, the zero level of the sensor output depends on the ambient temperature. The problem is caused by expansion of the air in the sensor cavity [9]. For monitoring pressures *in vivo* (i.e., in a human body or in an animal), the temperature change can be neglected but careful calibration is required before monitoring in a medium the temperature of which is the same as that of the monitoring area. To avoid thermal drift, a packaging process using soldering to keep the sensor cavity in vacuum has been proposed and the development is on going [15]. Such an absolute sensor will be necessary for long-term monitoring.

Considering the sensitivity of the sensor, the low visibility of the reflection spectrum of the sensor, shown in figure 7, degrades the sensitivity. The extent of the light beam from the multimode fiber end at the sensor causes the geometric path difference and degrades the sensitivity. Although making the cavity length of the sensor small (about 2 μm in our sensor) reduces the effect of the path difference, it limits the increase of sensitivity because of the large numerical aperture (NA) of the multimode fiber. Consequently, utilizing a single-mode fiber the NA of which is smaller than that of the multimode fiber can increase the sensitivity. Moreover, the beam diameter of the light from the single-mode fiber end is smaller. Therefore, a smaller mirror and a larger deformable area of the diaphragm can be designed to improve the sensitivity of the sensor. The fabrication process is exactly the same because the multimode and the single-mode fibers have the same outer diameter.

For clinical use, the sensor must be packaged in suitable medical tools (e.g., catheter, guide wire, needle) depending on the purpose. This sensor can be packaged in small medical tools because the diameter of the sensor is extremely small. Furthermore, it is an advantage that the function of the tools can be maintained even though the pressure sensor is embedded in one. We will examine not only fundamental sensor characteristics (e.g., thermal drift) but the packaging and the biocompatibility as well. In particular, the surface of the pressure sensor should be coated with suitable material to achieve biocompatibility for long-term monitoring.

From an economical viewpoint, even the spectrometer, which is the most expensive component in the sensor system, is available at a comparable price to a normal laptop PC. Consequently, the sensor system can be provided at a relatively low cost.

7. Conclusion

We have developed an ultra-miniature fiber-optic pressure sensor system for medical applications. The diameter of the sensor is 125 μm. A Fabry–Perot cavity is formed at the optical fiber end and a deformation of the diaphragm induced by pressure varies the cavity length. The sensing element is bonded to the optical fiber end utilizing a ring-shaped polyimide layer. White light interferometry is adopted to reduce error and noise caused by bending of the optical fiber and fluctuation of the light source. A measurement system for detecting the cavity length of the sensor has been developed. The system directly detects the modulated spectrum of the reflection light from the sensor interferometer using a commercial high-speed spectrometer. By tracking the shift of the peak wavelengths of the spectrum, the cavity length is calculated and the measured pressure is continuously displayed. Pressure has been successfully monitored in the heart and artery of a goat in real time using the developed sensor system.

Because of the ultra-miniature sensor head, this sensor can be used in a small-diameter blood vessel or a stenosed vessel. It can also be utilized for multi-point measurement at the same time by setting more than one sensor in a tool. Furthermore, the sensor is expected to be useful in multi-functional interventional tools.

Acknowledgments

The authors would like to thank Professor T Yambe and Dr Y Shiraishi for help with experiments on animals. This work was supported in part by a Health and Labour Science Research Grants (Research on Advanced Medical Technology) from the Ministry of Health, Labour and Welfare of Japan. The authors acknowledge the support of Tohoku University 21COE Program 'Future Medical Engineering Based on Bio-nanotechnology'.

References

[1] Wolthuis R A, Mitchell G L, Saaski E, Hartl J C and Afromowitz M A 1991 Development of medical pressure and temperature sensors employing optical spectrum modulation *IEEE Trans. BME* **38** 974–81

[2] Kalvesten E, Smith L, Tenerz L and Stemme G 1998 The first surface micromachined pressure sensor for cardiovascular pressure measurements *Proc. 11th IEEE Micro Electro Mechanical Systems (Heidelberg, Germany, 1998)* pp 574–9

[3] Tohyama O, Kohashi M, Sugihara M and Itoh H 1998 A fiber-optic pressure microsensor for biomedical applications *Sensors Actuators* A **66** 150–4

[4] Melvas P, Kalvesten E and Stemme G 2002 A temperature compensated dual beam pressure sensor *Sensors Actuators* A **100** 46–53

[5] Abeysinghe D C, Dasgupta S, Jackson H E and Boyd J T 2002 Novel MEMS pressure and temperature sensor fabricated on optical fiber *J. Micromech. Microeng.* **12** 229–35

[6] Rao Y J and Jackson D A 1994 A prototype fibre-optic-based Fizeau medical pressure and temperature sensor system using coherence reading *Meas. Sci. Technol.* **5** 741–6

[7] Haga Y, Minami K, Shoji S, Nitta S, Tanaka M and Esashi M 1994 A fiber-optic ultra miniature pressure sensor *Proc. 12th Sensor Symp. (Osaka, Japan, 1994)* pp 135–8

[8] Katsumata T, Haga Y, Minami K and Esashi M 2000 Micromachined 125 μm diameter ultra miniature fiber-optic pressure sensor for catheter *Trans. IEEJ* **120-E** 58–63

[9] Totsu K, Minh P N, Haga Y and Esashi M 2002 Development of ultra miniature fiber-optic blood pressure sensor system *Proc. 19th Sensor Symp. (Kyoto, Japan, 2002)* pp 429–32

[10] Bhatia V, Sen M B, Murphy K A and Claus R O 1996 Wavelength-tracked white light interferometry for highly sensitive strain and temperature measurements *Electron. Lett.* **32** 247–9

[11] Belleville C and Duplain G 1993 White-light interferometric multimode fiber-optic strain sensor *Opt. Lett.* **18** 78–80

[12] Rao Y J and Jackson D A 1996 Recent progress in fibre optic low-coherence interferometry *Meas. Sci. Technol.* **7** 981–99

[13] Chen S, Palmer A W, Grattan K T V and Meggitt B T 1992 Digital signal-processing techniques for electronically scanned optical-fiber white-light interferometry *Appl. Opt.* **31** 6003–10

[14] Lee C E and Taylor H F 1991 Fiber-optic Fabry–Perot temperature sensor using a low-coherence light source *J. Light. Technol.* **9** 129–34

[15] Totsu K, Haga Y and Esashi M 2003 Vacuum sealed ultra miniature fiber-optic blood pressure sensor using white light interferometry *Digest of Technical Papers of the 12th Int. Conf. on Solid State Sensors, Actuators and Microsystems: Transducers'03 (Boston, MA, 2003)* pp 931–4

JOURNAL OF APPLIED PHYSICS 97, 1 (2005)

Synchronous rectification for contactless power supply utilizing Mn–Zn ferrite core coils

Hidekazu Miura,[a] Shinsuke Arai, Fumihiro Sato, and Hidetoshi Matsuki
Graduate School of Engineering, Tohoku University, 6-6-05aza Aoba Aramaki Aoba ward Sendai, Miyagi 980-8579 Japan

Tadakuni Sato
NEC Tokin corporation

(Presented on 11 November 2004)

Contactless power supply systems transmit electric power by electromagnetic induction with a pair of coils. The efficiency and the output voltage depend on parameters of coils. We studied the best parameter values that realize stable high efficiency contactless power supply. In the application with low output voltage, the voltage drop of the diodes becomes dominant power loss. A synchronous rectification was proposed as a solution of this problem. Our contactless power supply system for an artificial heart operates at 190 kHz. We use planar coils with Mn–Zn ferrite cores. Highly stable output voltage and 88% maximum efficiency were realized. © *2005 American Institute of Physics.*
[DOI: 10.1063/1.1850852]

I. INTRODUCTION

Contactless power supply systems transmit electric power by electromagnetic induction with a pair of coils. The systems are applied to wireless power supply method for artificial organs to prevent recipients from infection syndromes and restraint of actions. We call thus a transcutaneous energy transmission system, TETS.[1,2] Also contactless power supply systems will make underwater vehicles free from wire and connectors. And we can use waterproof electronic product such as cellar phones or shavers.[3] The efficiency and the output voltage depend on parameters of self-inductance L and mutual inductance M of the coil. We studied the best parameter values that realize stable high efficiency contactless power supply. In the application with low output dc voltage, the voltage drop of the diodes becomes a problem of the loss. A synchronous rectification was proposed as a solution to this problem.

II. DETERMINATION OF CIRCUIT PARAMETERS

Figure 1 shows the equivalent circuit of contactless power supply system. If the operating frequency is decided, the efficiency is calculated from the equivalent circuit

$$= \frac{R}{\dfrac{r_1 \; r_2+R\;^2+\;^2L_2^2}{^2M^2} + r_2+R}.$$

L, M, and r depend on the number N of windings of coils. If we make coils with the uniform cross sections of coils, we can assume each parameter proportional to the square of N, then the efficiency is shown as functions of the number T of windings of the secondary coil C_2=0 . The term, n is the ratio of the winding number of the primary coil to the secondary coil. L and L are the values of one-turned self-inductances for the primary coil, and the secondary coil respectively. And r and r are the values of one-turned wire wound resistances for the primary coil and the secondary coil, respectively

$$L_1 = n^2T^2L,$$

$$L_2 = T^2L\,,$$

$$r_1 = n^2T^2r,$$

$$r_2 = T^2r\,,$$

$$N_1 = nT.$$

T, by which efficiency is assumed to be the maximum, is decided from this expression

$$T^4 \frac{rR^2}{r\;\;^2k^2LL\;^2+rr+r\;\;^2k^2LL}.$$

The transformer formed by the coils is a loose-coupled one. This results in high output impedance and output variance. We use resonant capacitor C_1 in series. C_1 that minimizes internal impedance Z_0 is determined and the change of output voltage is suppressed when the load changes. In Fig. 2, the Helmholtz equivalent circuit is shown. In most cases, wire wound resistances r_1 and r_2 are negligible for output voltage considerations. C_1 is determined by

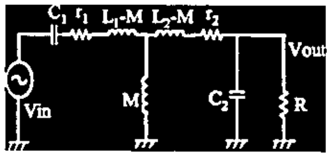

FIG. 1. Equivalent circuit of contactless power supply system.

[a]Author to whom correspondece should be addressed; electronic mail: biomg26@ec.ecei.tohoku.ac.jp

